ISSN 1063-7834, Physics of the Solid State, 2016, Vol. 58, No. 5, pp. 924–932. © Pleiades Publishing, Ltd., 2016.
Original Russian Text © V.V. Bannikov, A.R. Beketov, M.V. Baranov, A.A. Elagin, V.S. Kudyakova, R.A. Shishkin, 2016, published in Fizika Tverdogo Tela, 2016, Vol. 58, No. 5, pp. 897–904.

SEMICONDUCTORS

Electronic Structure and Magnetic Properties of Doped $Al_{1-x}Ti_xN$ ($x = 0.03, 0.25$) Compositions Based on Cubic Aluminum Nitride from Ab Initio Simulation Data

V. V. Bannikov[a, *], A. R. Beketov[b], M. V. Baranov[b], A. A. Elagin[b], V. S. Kudyakova[b], and R. A. Shishkin[b]

[a] *Institute of Solid State Chemistry, Ural Branch of the Russian Academy of Sciences, ul. Pervomaiskaya 91, Yekaterinburg, 620990 Russia*

[b] *Ural Federal University named after the First President of Russia B. N. Yeltsin, ul. Mira 19, Yekaterinburg, 620002 Russia*

** e-mail: bannikov@ihim.uran.ru*

Received June 30, 2015; in final form, November 16, 2015

Abstract—The phase stability, electronic structure, and magnetic properties of $Al_{1-x}Ti_xN$ compositions based on the metastable aluminum nitride modification with the rock-salt structure at low ($x = 0.03$) and high ($x = 0.25$) concentrations of titanium in the system have been investigated using the results of ab initio band calculations. It has been shown that, at low values of x, the partial substitution is characterized by a positive enthalpy, which, however, changes sign with an increase in the titanium concentration. According to the results of the band structure calculations, the doped compositions have electronic conductivity. For $x = 0.03$, titanium impurity atoms have local magnetic moments (~0.6 μ_B), and the electronic spectrum is characterized by a 100% spin polarization of near-Fermi states. Some of the specific features of the chemical bonding in $Al_{1-x}Ti_xN$ cubic phases have been considered.

DOI: 10.1134/S106378341605005X

1. INTRODUCTION

Aluminum nitride exhibits a unique combination of physical characteristics that are important for practical applications: the wide band gap (up to 6.2 eV), high electrical resistivity (~10^{13} Ω cm), high thermal conductivity (to 320 W/(m K) for single crystals and 180–220 W/(m K) for sintered powders), high Vickers hardness (12 GPa) [1], chemical resistance in the bulk state, and nontoxicity. Owing to the aforementioned properties, aluminum nitride is a very promising material for applications in many branches of industry, such as the manufacture of micro-modules, integrated circuits, active elements of light-emitting diodes, and thermally conductive composite materials (fillers), metallurgy (lining materials for electrolysis cells, tanks, crucibles for molten aluminum, tin, gallium, glass, etc.), atomic industry (due to the high corrosion resistance to molten salt media, AlN coatings can be used for functional and structural components of nuclear reactors), and space engineering (housings and substrates for powerful monolithic integrated circuits of power amplifiers, thermally conductive insulators for heaters of active instrument thermostats, substrates for thermoelectric converters based on Peltier elements in systems for cooling to the temperature of 160 K) [1–3].

There are several known crystalline modifications of aluminum nitride [4]: the most stable (and well-studied) modification has a hexagonal lattice of the wurtzite type (*w*-AlN), while the known metastable phases have cubic structures of the sphalerite (*s*-AlN) and rock salt (*r*-AlN) types. Of particular interest is the metastable modification *r*-AlN, because it has a higher thermal conductivity (250–600 W/(m K) for sintered powders) as compared to the hexagonal modification *w*-AlN (due to the higher symmetry of the crystal lattice and, therefore, the weaker phonon scattering [5, 6]), the high electrical resistivity (~10^{16} Ω cm) and mechanical strength [7], as well as wide band gap (the experimentally determined minimal value of the band gap corresponding to the indirect optical transition for thin films is equal to 3.83 eV, according to the data reported in [6], or 4.81 eV [8]).

At present, there is a sufficient number of studies devoted to theoretical simulation of the band structure as well as the elastic, electronic, optical, and thermodynamic properties of the AlN cubic phases in the bulk state (see, for example, [8–23]). In particular, it was

shown that (1) both cubic modifications, *s*-AlN and *r*-AlN, are mechanically stable; (2) the cubic modification *r*-AlN is stabilized with respect to the hexagonal modification *w*-AlN at an external pressure of higher than ~13 GPa; (3) according to the results of the simulation of the *P*–*T* phase diagram for AlN, the minimal pressure stabilizing the *r*-AlN phase decreases with an increase in the temperature; and (4) in contrast to the *w*-AlN compound, which is a direct-band-gap semiconductor, for the *s*-AlN and *r*-AlN phases, the minimal values of the band gaps correspond to the indirect Γ–*X* electronic transition and amount to 3.2–3.4 and 4.0–4.5 eV, respectively. However, it should be noted that the studies on the synthesis of metastable cubic phases of aluminum nitride AlN and their physical characteristics (see, for example, [4–6, 8, 14, 24–32]), as a rule, have dealt with the properties of thin films, coatings, nanoparticles, or powder materials. As a result, it remains an open problem whether they can be synthesized in the form of bulk samples certainly of interest for practical applications. An approach proposed in [14, 33, 34] to the synthesis of the *r*-AlN phase consisted in the isostructural spinodal decomposition of metastable solid solutions with the $Ti_{1-x}Al_xN$ composition (for example, $Ti_{0.6}Al_{0.4}N$) into aluminum and titanium cubic nitrides. The authors of these papers assumed that the binary phases formed upon decomposition are free of impurities and stoichiometric. At the same time, under certain conditions (for example, with excess of titanium in the system), the formation of doped cubic aluminum nitrides $r\text{-}Al_{1-x}Ti_xN$ with low titanium concentrations $x \sim 0.01$–0.05 seems to be quite probable, because the atomic radii of Al and Ti are close enough to each other ($R_{Al} = 1.43$ Å, $R_{Ti} = 1.46$ Å). Therefore, it can be expected that the partial substitution of titanium for aluminum in the lattice of the *r*-AlN phase, which, at small concentrations, is accompanied only by local distortions of the crystal structure, can occur with a low consumption of energy. In this case, the electronic, transport, magnetic, thermodynamic, and other properties of titanium lightly doped phases based on *r*-AlN can differ significantly from the properties of undoped aluminum nitride and $Ti_{1-x}Al_xN$ solid solutions with high concentrations $x \sim 0.25$–0.75, which were studied in the majority of works known to the authors. In our opinion, the prediction of the physical properties of impurity compositions $r\text{-}Al_{1-x}Ti_xN$ with low concentrations *x* and the evaluation of their phase stability seem to be a useful step in the development of the theoretical basis for the efficient synthesis and technological applications of the cubic modification of aluminum nitride.

In this work, based on the results of ab initio band calculations, we have carried out a comparative study of the phase stability, electronic structure, and magnetic properties of the doped composition $r\text{-}Al_{1-x}Ti_xN$ for two specific cases of low ($x = 0.03$) and high ($x = 0.25$) titanium impurity concentrations. The first case simulates the formation of single titanium impurity centers in the cubic aluminum nitride, which is accompanied by a local transformation of the crystalline environment, whereas the second case simulates the formation of an ordered solid solution in which Al and Ti atoms are in equivalent positions of the initial face-centered cubic (fcc) lattice of aluminum nitride, and the interatomic distances Al–N and Ti–N are equal to each other.

2. MODELS AND COMPUTATIONAL ASPECTS

The cubic modification of the aluminum nitride *r*-AlN has the rock-salt structure with the lattice constant varying for thin films in the range from 4.06 to 4.045 Å [4, 9, 32, 34] depending on the synthesis conditions. The doped phase $r\text{-}Al_{1-x}Ti_xN$ at the titanium concentration $x = 0.03$ was simulated by an extended $2 \times 2 \times 2$ supercell of $Al_{31}TiN_{32}$ (the central aluminum atom was replaced by the titanium atom) corresponding to the nominal composition $Al_{0.97}Ti_{0.03}N$, whereas at $x = 0.25$, the phase was simulated by an Al_3TiN_4 cell obtained from the conventional cell of *r*-AlN by the replacement of aluminum atoms at the cube vertices by titanium atoms and corresponding to the nominal composition $Al_{0.75}Ti_{0.25}N$ (Fig. 1). Both of the chosen cells possess the symmetry of the simple cubic lattice (space group *Pm*-3*m*).

The energies and band structures of all the compounds under consideration were calculated using the full-potential linearized augmented plane wave (FP-LAPW) method (spin-polarized version) with the generalized gradient approximation (GGA) for the exchange–correlation potential in the Perdew–Burke–Ernzerhof (PBE) form [35] implemented in

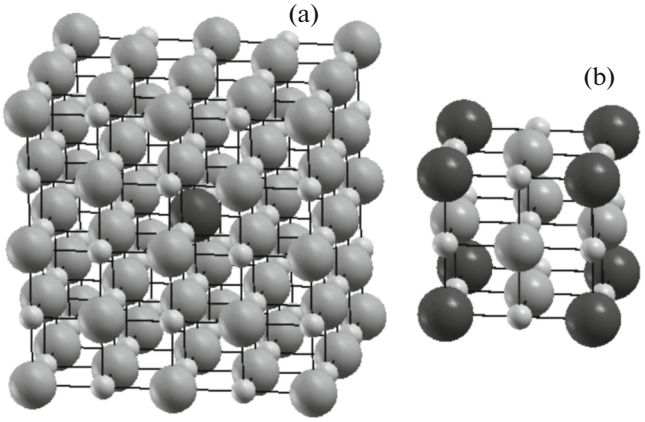

Fig. 1. Cubic cell simulating the doped $r\text{-}Al_{1-x}Ti_xN$ phase with titanium concentrations x = (a) 0.03 ($Al_{31}TiN_{32}$) and (b) 0.25 (Al_3TiN_4). Large black and gray balls are titanium and aluminum atoms, respectively. Small balls are nitrogen atoms.

Crystal structure type, the optimized lattice constants (a and c in Å), the number of formula units per unit cell (Z), and the ground-state energy (E, in Ry) per formula unit of the considered phases according to the data of ab initio calculations

Compound	Structure	a, c	Z	E
Ti	hcp	2.978	2	−1707.618454
	($P6_3/mmc$)	4.678		
Al	fcc	4.032	1	−485.641256
	(Fm-3m)	–		
TiN	fcc	4.248	1	−1817.410499
	(Fm-3m)	(4, 256[a])		
		4.235, 4.250[b]		
r-AlN	fcc	4.071	1	−595.342673
	(Fm-3m)	(4.070[a], 4.001[c],		
		3.982[d], 4.068[e])		
		–		
$Al_{31}TiN_{32}$	pc	8.142	1	−20272.900327
	(Pm-3m)	–		
Al_3TiN_4	pc	4.136	1	−3603.350149
	(Pm-3m)	–		

Data taken from the following papers: [a] [8], [b] [38], [c] [9], [d] [17], and [e] [19] (see also [20–22] and references therein).

the WIEN2k software package [36]. The radii of the atomic muffin-tin (MT) spheres for all phases were chosen as follows: 1.8 bohr for Al, Ti and 1.5 bohr for N. The plane-wave basis set was limited by the value K_{max} determined as the $R_{MT} \times K_{max} = 7.0$, where R_{MT} is the minimal value of the chosen atomic MT radii, $E_{cut\text{-}off} = 6.0$ Ry is the energy separating the core electron states from the valence states, and $E_{l=2}(\text{Ti}) = 0.50$ Ry is the linearization energy for the d states of titanium atoms. The integration over the Brillouin zone was performed by the tetrahedron method [37] using a $10 \times 10 \times 10$ k-point grid. The convergence criteria for self-consistent calculations were as follows: 0.01 mRy for the total energy, 0.001 e for the electron charge, and 1 mRy/bohr for the forces acting on the atomic cores.

3. RESULTS AND DISCUSSION

3.1. Phase Stability

At the first stage of our investigation, we optimized the structural parameters and calculated the energies of the equilibrium state of the r-AlN and TiN nitrides with the rock-salt structure, as well as metallic aluminum and titanium (in the most stable modifications, fcc and hexagonal close-packed (hcp), respectively). The obtained results are presented in the table. It can be seen that they are in satisfactory agreement with the available experimental and theoretical data. It is interesting to note that the lattice constant of 4.071 Å for r-AlN in the bulk state is very close to the experimentally determined value of 4.08 Å for aluminum nitride films in the epitaxial layer structures r-AlN/TiN [4]. This circumstance allows us to hope that physical properties (electronic, transport, mechanical, etc.) of the bulk phase and cubic aluminum nitride thin films grown on TiN substrates will also be largely similar to each other. According to the obtained data, the enthalpy $\Delta H = \Delta E + P\Delta V$ for the formal reaction of the complete substitution of titanium for aluminum r-AlN + Ti → TiN + Al at $P = 0$ and $T = 0$ K is negative and equal to approximately −1.233 eV/form.unit, thus indicating the preference of the replacement Ti → Al in the cubic structure of the nitride. At the same time, in the case of a partial substitution, the formation of isolated titanium impurity centers in r-AlN can be accompanied by the energy consumption associated with local distortions of the crystal structure, because the Al–N and Ti–N equilibrium distances in the cubic nitrides are slightly different from each other (2.035 and 2.124 Å, respectively).

In order to investigate the phase stability of the r-$Al_{1-x}Ti_xN$ system at different impurity concentrations, we carried out the structural optimization of the compound with the formal composition $Al_{31}TiN_{32}$, which simulated single titanium impurity centers in the lattice of the r-AlN phase, and the Al_3TiN_4 compound simulating the solid solution at $x = 0.25$ (Fig. 1). In the first case, it was assumed that the lattice constant of the $Al_{31}TiN_{32}$ compound is equal to twice the lattice constant for r-AlN, and the change in the crystal structure is determined only by the relaxation of atoms from the coordination spheres nearest to the titanium impurity. This simplification seems to

be reasonable, because, according to the results of the optimization, the displacement of the six nitrogen atoms nearest to the titanium impurity from the initial positions (the first coordination sphere) is equal to ~0.06 Å, whereas the displacement of twelve nearest neighbor aluminum atoms to a new equilibrium position (the second coordination sphere) is already one order of magnitude smaller, and the displacements of atoms from more distant coordination spheres are insignificant. In the second case, we assumed that all the atoms in the Al_3TiN_4 cell are located in fixed crystallographic positions (the Al–N and Ti–N interatomic distances are equal to each other), and the optimization was reduced to the determination of the equilibrium value of the lattice constant (4.136 Å). The calculated energies of the optimized structures $Al_{31}TiN_{32}$ and Al_3TiN_4 are presented in the table. Based on the obtained results, it is easy to estimate the enthalpies ΔH for the formal partial substitution reactions

$$32r\text{-AlN} + \text{Ti} \rightarrow Al_{31}TiN_{32} + \text{Al}$$

and

$$4r\text{-AlN} + \text{Ti} \rightarrow Al_3TiN_4 + \text{Al}$$

(also at $P = 0$ and $T = 0$ K), which are approximately equal to +0.577 and –0.031 eV, respectively (or +0.018 and –0.008 eV per formula unit of the $Al_{0.97}Ti_{0.03}N$ and $Al_{0.75}Ti_{0.25}N$ compositions, respectively).

Thus, although the enthalpy of formation of the doped r-$Al_{0.97}Ti_{0.03}N$ phase is positive, its absolute value is relatively small (~5% of the energy of the transition of the aluminum nitride AlN from the wurtzite-like phase to the r-AlN phase, which, according to estimates [9, 10], lies in the range of ~0.32–0.34 eV/form.unit). Therefore, we can expect that, at sufficiently high temperatures, the entropy contribution to the change in the Gibbs free energy $\Delta G = \Delta H - T\Delta S$ will exceed the aforementioned enthalpy ΔH and thus will lead to the value of $\Delta G < 0$. Consequently, the formation of titanium lightly doped r-$Al_{1-x}Ti_xN$ phases containing single impurity centers seems to be quite probable. It is interesting to note that the enthalpy of formation of the r-$Al_{0.75}Ti_{0.25}N$ phase has a negative value. This indicates the possibility of the partial substitution reaction Ti → Al in r-AlN with the formation of an ordered solid solution even at $T = 0$ K, whereas the absolute value of the enthalpy of formation is relatively low. Hence, it can be expected that the direction of this reaction, as in the previous case, will depend substantially on the conditions of its occurrence. The slightly smaller value of ΔH for the r-$Al_{0.75}Ti_{0.25}N$ phase, as compared to r-$Al_{0.97}Ti_{0.03}N$, can most likely be explained by the formation of additional covalent Ti–N bonds in the crystal (see below), which stabilize the system. At the same time, as noted in [34], the $Ti_{1-x}Al_xN$ solid solutions are metastable with respect to the isostructural decomposition into the cubic nitrides AlN and TiN, because the calculated enthalpies of isostructural mixing over the entire range of concentrations x are positive and reach the maximum at $x \sim 0.7$. Therefore, the enthalpy of the formal reaction of decomposition of the r-$Al_{0.97}Ti_{0.03}N$ phase into r-AlN and TiN will be all the more positive. It should be noted, however, that owing to distortions of the crystal structure of this phase due to the relaxation of atoms in the nearest environment of the impurity centers, this decomposition is no longer isostructural and may spontaneously not occur for kinetic reasons (for example, due to the high energy of the intermediate state of the system). However, the solution of this problem goes far beyond the scope of this paper. Therefore, we will restrict ourselves to general remarks that the formation of the metastable r-$Al_{0.97}Ti_{0.03}N$ phase (for example, in a mixture of metallic titanium and r-AlN) is characterized by a not too high value of the enthalpy and, at reasonable temperatures, seems to be quite probable, along with the formation of $Al_{1-x}Ti_xN$ solid solutions with titanium concentrations $x \geqslant 0.25$.

3.2. Electronic Structure and Magnetic Properties

To date, there is quite a lot of papers devoted to the theoretical study of the band structure of the nitrides TiN and r-AlN (defect-free cubic crystals). Therefore, we will discuss its specific features only briefly. Figure 2 presents the total and partial densities of electronic states (DOS) for the aforementioned nitrides and the structure of the energy bands $E(k)$ for the aluminum nitride r-AlN, which were calculated for their equilibrium crystal structure and are in reasonable agreement with the results reported in [38, 39] for TiN and in [10, 18–23, 33, 34] for r-AlN. It can be seen that r-AlN is a wide-band-gap semiconductor, and the top of the valence band and the bottom of the conduction band correspond to the Γ and X points of the Brillouin zone, respectively. The minimal band gap corresponds to the indirect Γ–X optical transition and, according to the calculations, amounts to ~4.35 eV. This value is in satisfactory agreement with the results presented in the papers [18–23], which reported values in the range of 4.0–4.5 eV. For the direct Γ–Γ transition, the calculated band gap is ~5.38 eV. As is known, one of the drawbacks of the methods used for band structure calculations and based on the density functional theory (DFT) is a systematic underestimation of the band gap of the material as compared to the experimental value [40]. At the same time, as far as we know, there are only two papers devoted to the experimental determination of the band gap in r-AlN, where the values of the band gap were found to be 3.83 eV [6] and 4.81 eV [8], which are in relatively good agreement with the calculated data. However, it should be remembered that the estimates were made for the bulk state, whereas the authors of [6, 8] were dealing with r-AlN thin films, and the band gaps for these two forms of the

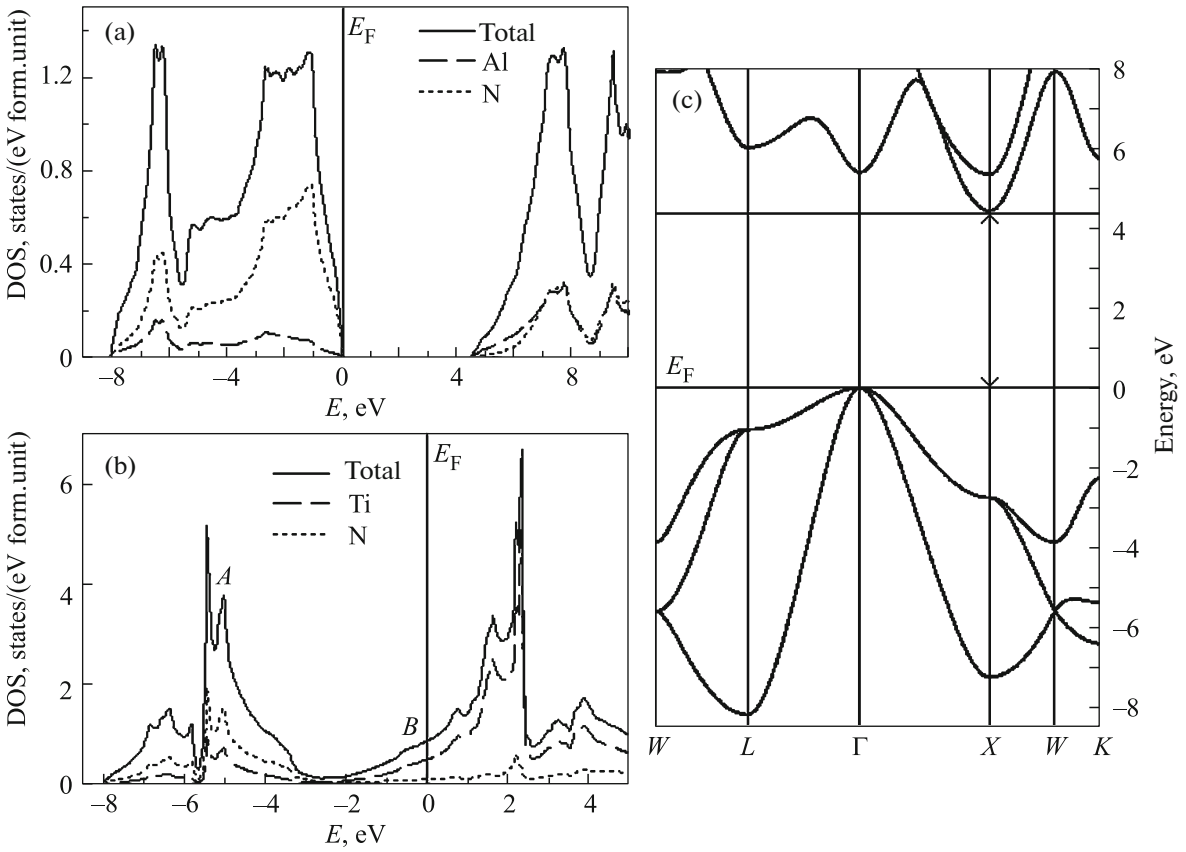

Fig. 2. Total and partial densities of electronic states for cubic nitrides: (a) *r*-AlN and (b) TiN (see text). (c) Structure of the energy bands $E(k)$ for *r*-AlN. In all cases, the position of the Fermi level (E_F) is taken as zero.

same material can differ significantly (for example, the experimental value of the band gap for bulk MgO single crystals is equal to ~7.77 eV [41], while for thin films, it can be ~2.5 eV [42]). As can be seen from Fig. 2, the valence band of *r*-AlN is predominantly formed by the N–2*p* states with a relatively small (especially near the top of the valence band) contribution from the aluminum states, whereas the contributions from these states to the formation of the bottom of the conduction band are comparable to each other. As regards the titanium nitride, its electronic spectrum consists of two main bands: (1) the *A* band located ~(3–8) eV below the Fermi level (E_F) and formed by the hybridized N–2*p* and Ti–3*d* states (Fig. 2) responsible for the formation of the covalent components of the chemical bonds Ti–N; and (2) the *B* band with the near-Fermi part formed only by the Ti–3*d* states (with the calculated density at E_F: $N(E_F)$ = 0.86 states/(eV form. unit)) responsible for metallic conductivity of TiN. The spin polarization of "spin-up" and "spin-down" electronic states for both nitrides is negligible, and their ground state is nonmagnetic.

A completely different situation occurs with the impurity phase *r*-$Al_{0.97}Ti_{0.03}N$. Figure 3 shows the density-of-state distributions calculated for the optimized structure of the formal composition $Al_{31}TiN_{32}$. As can be seen from this figure, the incorporation of titanium atoms into the *r*-AlN structure leads to the appearance of the impurity Ti–3*d* band in the electronic spectrum, which undergoes an orbital splitting into the t_{2g} and e_g components in the cubic crystal, so that the t_{2g} band appears to be lying in the band gap of the initial matrix and partially filled, whereas the e_g band merges with the bottom of its conduction band and remains vacant. In turn, the impurity Ti–t_{2g} and Ti–e_g bands undergo spontaneous spin polarization due to the intra-atomic exchange in the partially filled Ti–3*d* shell, thus splitting into the spin components Ti–$t_{2g\uparrow,\downarrow}$ and Ti–$e_{g\uparrow,\downarrow}$ respectively. As a result, the Ti–$t_{2g\uparrow}$ band crosses the Fermi level E_F and is partially filled, while the Ti–$t_{2g\downarrow}$ band is vacant (Figs. 3, a2). This is accompanied by the formation of local magnetic moments of ~0.63 μ_B at titanium impurity atoms (the values were calculated within the corresponding MT spheres), the magnetic moments of the other atoms do not exceed the absolute value of ~10^{-3} μ_B, and the complete magnetic moment per cell of the formal composition $Al_{31}TiN_{32}$ is close to an integer value of ~1 μ_B. Thus,

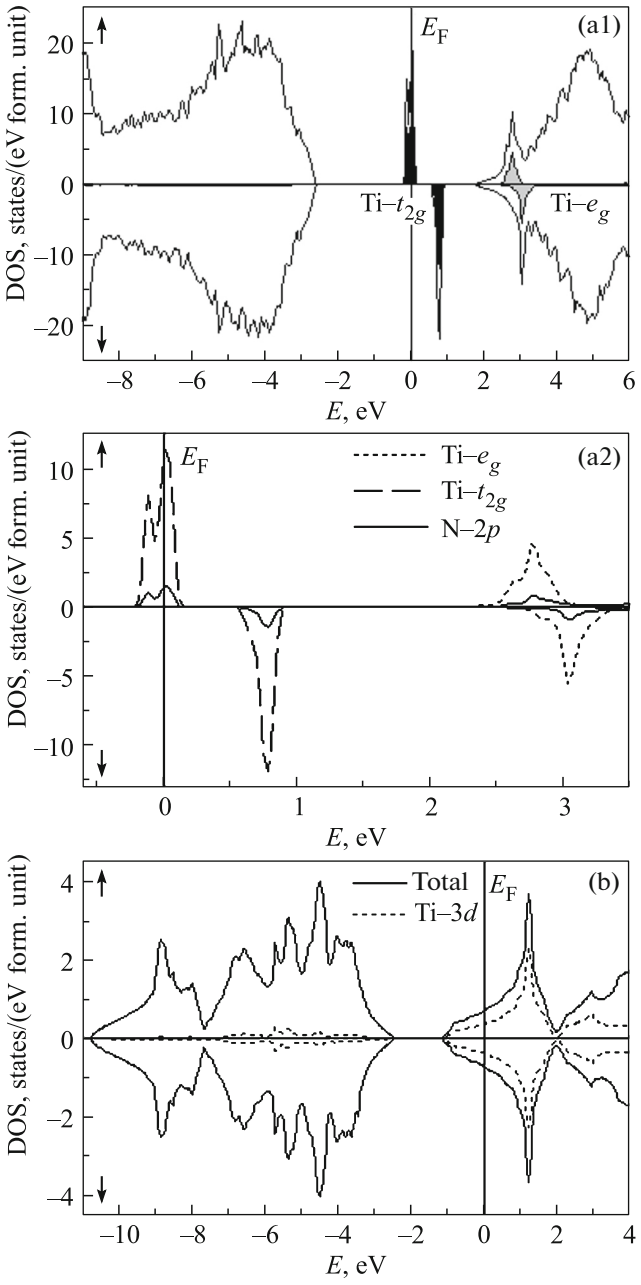

Fig. 3. Densities of electronic states for impurity systems (a) $Al_{31}TiN_{32}$ (r-$Al_{0.97}Ti_{0.03}N$): (a1) the survey spectrum and (a2) the impurity Ti($3d$)–t_{2g} and Ti($3d$)–e_g states in the band gap of the initial matrix (r-AlN); and (b) Al_3TiN_4 (r-$Al_{0.75}Ti_{0.25}N$).

the impurity phase r-$Al_{0.97}Ti_{0.03}N$ becomes conductive and, according to the results of the simulation of the band structure, is characterized by a 100% spin polarization of the near-Fermi electronic states $P = |N_\uparrow(E_F) - N_\downarrow(E_F)|/[N_\uparrow(E_F) + N_\downarrow(E_F)]$ (according to our calculations, for the phase of the formal composition $Al_{31}TiN_{32}$, the density of states at the Fermi level $N_\uparrow(E_F) = 22.20$ states/(eV form.unit), $N_\downarrow(E_F) = 0$). This phase is conductive with respect to only one electron spin subsystem (for definiteness, "spin up") and represents a semiconductor with respect to the other subsystem ("spin down," see also [43]). In this context, we can mention the paper of Wu et al. [44], who carried out the simulation of the band structure of the partially magnesium substituted wurtzite-like phase w-$Al_{0.9375}Mg_{0.0625}N$ (with the formal composition $Al_{15}MgN_{16}$), for which the authors also predicted a 100% spin polarization of the near-Fermi states.

As regards the Al_3TiN_4 system, which simulates the r-$Al_{0.75}Ti_{0.25}N$ solid solution, an increase in the titanium concentration leads, on the one hand, to a significant broadening of the near-Fermi band predominantly formed by the Ti–3d states (Fig. 3) and, on the other hand, to the absence of its spin polarization (the calculated magnetic moments of both the individual atoms and the Al_3TiN_4 cell as a whole are negligible). This fact can be qualitatively explained by taking into account the simplest Stoner criterion for ferromagnetism of electron gas $N(E_F) \cdot I > 1$ (where I is the parameter of electron–electron exchange interaction), as well as the decrease in the density of states at the Fermi level $N(E_F)$ (per formula unit of $Al_{1-x}Ti_xN$) about twice when going from $Al_{31}TiN_{32}$ to Al_3TiN_4. Therefore, the r-$Al_{0.75}Ti_{0.25}N$ solid solution is characterized as a conventional metal whose magnetic properties are determined by the Pauli paramagnetism of conduction electrons with the magnetic susceptibility $\chi = 2\mu_B^2 N(E_F)/3 \sim 7.4 \times 10^{-6}$ cm^3/mol (where $N(E_F) = 1.39$ states/(eV form.unit) is the calculated value per formula unit of Al_3TiN_4 and the factor of 2/3 is due to the Landau diamagnetism). Thus, according to the results of the simulation, upon incorporation of titanium impurity atoms into the cubic aluminum nitride, the impurity phase r-$Al_{1-x}Ti_xN$ acquires metallic conductivity. In this case, the impurity phase at low concentrations x (a few percent) can undergo a transition to the magnetic state, whereas at $x \sim 0.25$, it is a nonmagnetic metal.

Finally, we briefly consider specific features of the chemical bonding in the r-$Al_{1-x}Ti_xN$ phases in comparison with the perfect cubic aluminum nitride r-AlN. The maps of the charge density distributions in the corresponding planes parallel to the (100) plane for the r-AlN and titanium-containing cubic phases under consideration are shown in Fig. 4. It can be seen from this figure that, in r-AlN, there are almost no directional cation–anion Al–N bonds (Fig. 4a). In other words, the covalent component plays a minor role, and the chemical bonding has a pronounced ionic character. The effective atomic charges calculated according to the Bader scheme [45] are equal to $Q(Al) = +2.51e$ and $Q(N) = -2.51e$. These values are somewhat different from the values estimated in the formal ionic model: $Al^{3+}N^{3-}$. The incorporation of isolated titanium atoms into aluminum sites in the lat-

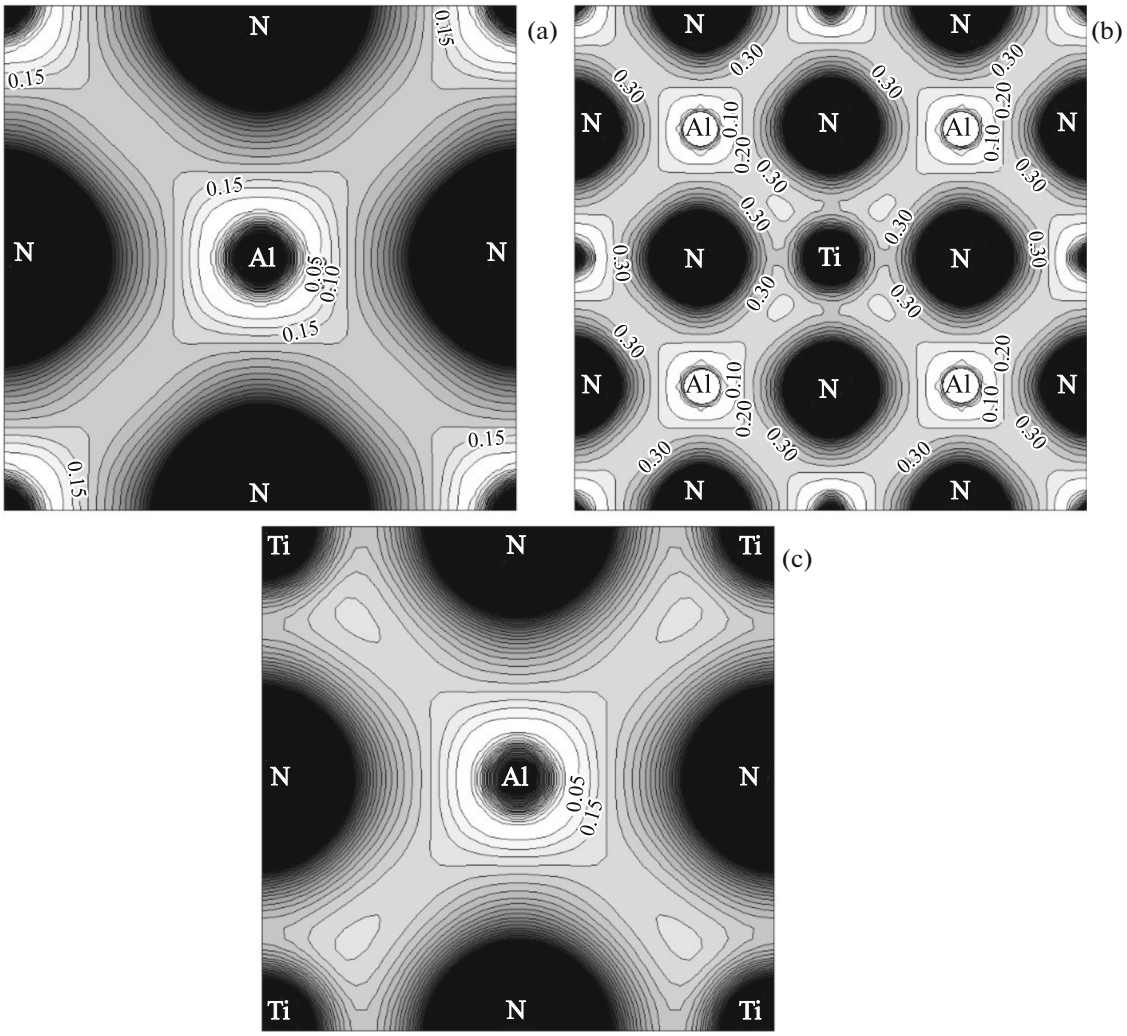

Fig. 4. Charge density distribution maps: (a) in the (100) plane of *r*-AlN, (b) in the (200) plane of $Al_{31}TiN_{32}$, and (c) in the (100) plane of Al_3TiN_4. The distances between the contours on maps (a, c) and (b) are equal to 0.05 and 0.10 $e/Å^3$, respectively.

tice of the *r*-AlN phase leads to the formation of directional bonds between the titanium atom and nitrogen atoms involved in its nearest environment (Fig. 4b, $x = 0.03$). It should be noted that the Ti–3*d* states in the *r*-$Al_{0.97}Ti_{0.03}N$ system, along with the formation of the near-Fermi Ti–t_{2g} band, are also admixed to a small extent with the valence band of the initial matrix composed predominantly of the N–2*p* states (in the range ~4 eV below the top of the valence band, see Figs. 2 and 3) and thus can participate in the formation of bonding electronic states in the crystal. A further increase in the titanium concentration leads to an increase in the contribution from the Ti–3*d* states to the low-lying valence band separated from the partially filled near-Fermi band by the energy gap (Fig. 3). Therefore, it can be expected that the role of the aforementioned states in the formation of bonding states will also increase. Indeed, as can be seen from Fig. 4c, in the *r*-$Al_{0.75}Ti_{0.25}N$ system, there are well-defined directional Ti–N bonds. Therefore, it can also be expected that the role of the covalent component of the chemical bonding in solid solutions will be enhanced with an increase in the titanium concentration x (because, in this case, the number of Ti–N bonds per formula unit of $Al_{1-x}Ti_xN$ increases). This fact is probably responsible for the stabilization of the *r*-$Al_{0.75}Ti_{0.25}N$ phase (a lower value of the enthalpy ΔH) with respect to the *r*-$Al_{0.97}Ti_{0.03}N$ phase. No directional Al–N bonds are observed in the *r*-$Al_{1-x}Ti_xN$ phases, as well as in the perfect cubic aluminum nitride.

4. CONCLUSIONS

The phase stability, electronic structure, and magnetic properties of compounds with the formal compositions $Al_{31}TiN_{32}$ and Al_3TiN_4 based on cubic aluminum nitride, which simulated titanium-doped

$Al_{1-x}Ti_xN$ cubic phases at low ($x = 0.03$, single defects) and sufficiently high ($x = 0.25$, the solid solution with a regular lattice) impurity concentrations, were investigated based on the results of the ab initio band calculations. It was shown that, in contrast to the solid solution with the titanium concentration $x = 0.25$, the $Al_{0.97}Ti_{0.03}N$ phase containing single defects is metastable with respect to the mixture of metallic titanium and cubic AlN, while the enthalpy of partial substitution of titanium for aluminum is relatively small, so that the formation of this phase seems to be quite probable. Upon doping with titanium, the $Al_{1-x}Ti_xN$ phases acquire electronic conductivity. In this case, it was predicted that the compounds with the titanium concentration $x = 0.03$ should have a band structure characterized by a 100% spin polarization of near-Fermi states, whereas at $x = 0.25$, they should be in the state of a conventional nonmagnetic metal. The chemical bonding in the perfect cubic aluminum nitride has a pronounced ionic character. However, with an increase in the concentration of titanium in the $Al_1 - {}_xTi_xN$ solid solutions, the role of the covalent component increases, which, in the authors' opinion, qualitatively explains the stabilization of the solid solution (negative enthalpy of partial substitution) at $x \sim 0.25$.

ACKNOWLEDGMENTS

This study was supported by the Ministry of Education and Science of the Russian Federation within the framework of the Russian Federal Target Program "Investigations and Elaborations in Priority Fields of the Development of the Scientific and Technological Complex of Russia for 2014–2020" in the direction "Industry of Nanosystems" (state contract no. 14.575.21.0006, unique project identifier RFMEFI57514X0006).

REFERENCES

1. H. O. Pierson, in *Handbook of Refractory Carbides and Nitrides* (Noyes, Park Ridge, New Jersey, United States, 1996), pp. 237–239.
2. A. W. Weimer, G. A. Cochran, G. A. Eisman, J. P. Henley, B. D. Hook, L. K. Mills, T. A. Guiton, A. K. Knudsen, N. R. Nicholas, J. E. Volmering, and W. G. Moore, J. Am. Ceram. Soc. **77**, 3 (1994).
3. A. W. Wemer, *Carbide, Nitride and Boride Materials: Synthesis and Processing* (Chapman and Hall, London, 1997), pp. 6–68.
4. A. Madan, I. W. Kim, S. C. Cheng, P. Yashar, V. P. Dravid, and S. A. Barnett, Phys. Rev. Lett. **78**, 1743 (1997).
5. R. Thapa, B. Saha, and K. K. Chattopadhyay, J. Alloys Compd. **475**, 373 (2009).
6. X.-P. Hao, M.-Y. Yu, D.-L. Cui, Q.-L. Wang, and M.-H. Jiang, J. Cryst. Growth **242**, 229 (2002).
7. V. Heiner and R. Heidrum, Patentschrift DD 292903 A5, Bundesrepublik Deutschland (1991).
8. Q. Zhong, S. Huang, Y. Fu, X. Shen, J. Zeng, and H. He, Appl. Mech. Mater. **633–634**, 52 (2014).
9. A. J. Wang, S. L. Shang, T. Du, Y. Kong, L. J. Zhang, L. Chen, D. D. Zhao, and Z. K. Liu, Comput. Mater. Sci. **48**, 705 (2010).
10. W. Feng, S. Cui, H. Hu, W. Zhao, and Z. Gong, Physica B (Amsterdam) **405**, 555 (2010).
11. F. Litimein, B. Bouhafs, Z. Dridi, and P. Ruterana, New J. Phys. **4**, 64.1 (2002).
12. W. J. Fan, M. F. Li, T. C. Chong, and J. B. Xia, J. Appl. Phys. **79**, 188 (1996).
13. S. Berrah, H. Abid, A. Boukortt, and M. Sehil, Turk. J. Phys. **30**, 513 (2006).
14. N. Norrby, H. Lind, G. Parakhonskiy, M. P. Johansson, F. Tasnadi, L. S. Dubrovinsky, N. Dubrovinskaia, A. Abrikosov, and M. Oden, J. Appl. Phys. **113**, 053515 (2013).
15. M. E. Shervin and T. J. Drummond, J. Appl. Phys. **69**, 8423 (1991).
16. A. Rubio, J. L. Corkill, M. L. Cohen, E. L. Shirley, and S. G. Louie, Phys. Rev. B: Condens. Matter **48**, 11810 (1993).
17. D. Fritsch, H. Schmidt, and M. Grundmann, Phys. Rev. B: Condens. Matter **67**, 235205 (2003).
18. Y. C. Cheng, X. L. Wu, J. Zhu, L. L. Xu, S. H. Li, and P. K. Chu, J. Appl. Phys. **103**, 073707 (2008).
19. X. Zhang, Z. Chen, S. Zhang, R. Liu, H. Zong, Q. Jing, G. Li, M. Ma, and W. Wang. J. Phys.: Condens. Matter. **19**, 425231 (2007).
20. W. Zhang, X.-R. Chen, L.-C. Cai, and Q.-Q. Gou, Commun. Theor. Phys. **50**, 990 (2008).
21. Z.-Y. Jiao, S.-H. Ma, and J.-F. Yang, Solid State Sci. **13**, 331 (2011).
22. N. E. Christensen and I. Gorczyca, Phys. Rev. B: Condens. Matter **47**, 4307 (1993).
23. P. E. Van Camp, V. E. Van Doren, and J. T. Devreese, Phys. Rev. B: Condens. Matter **44**, 9056 (1991).
24. M. Shahien, M. Yamada, T. Yasui, and M. Fukumoto, Mater. Trans. **54**, 207 (2013).
25. D. J. As and C. Mietze, Phys. Status Solidi A **210**, 474 (2013).
26. T. Schupp, G. Rossbach, P. Schley, R. Goldhahn, M. Roppischer, N. Esser, C. Cobet, K. Lischka, and D. J. As, Phys. Status Solidi A **207**, 1365 (2010).
27. M. Yu, X. Hao, D. Cui, Q. Wang, X. Xu, and M. Jiang, Nanotechnology **14**, 29(2003).
28. L. D.Wang and H. S. Kwok, Appl. Surf. Sci. **154–155**, 439 (2000).
29. L. Li, X. Hao, N. Yu, D. Cui, X. Xu, and M. Jiang, J. Cryst. Growth **258**, 268 (2003).
30. J. Wang, W. L. Wang, P. D. Ding, Y. X. Yang, L. Fang, J. Esteve, M. C. Polo, and G. Sanchez, Diamond Relat. Mater. **8**, 1342 (1999).
31. K. Sumitani, R. Ohtani, T. Yoshida, S. Mohri, and T. Yoshitake, Inst. Phys. Conf. Ser.: Mater. Sci. Eng. **24**, 012017 (2011).
32. Y. Fu, X. Li, Y. Wang, H. He, and X. Shen, Appl. Phys. A: Mater. Sci. Process. **106**, 937 (2012).

33. B. Alling, A. V. Ruban, A. Karimi, O. E. Peil, S. I. Simak, L. Hultman, and I. A. Abrikosov, Phys. Rev. B: Condens. Matter **75**, 045123 (2007).
34. B. Alling, T. Marten, I. A. Abrikosov, and A. Karimi, J. Appl. Phys. **102**, 044314 (2007).
35. J. P. Perdew, S. Burke, and M. Ernzerhof, Phys. Rev. Lett. **77**, 3865 (1996).
36. P. Blaha, K. Schwarz, G. K. H. Madsen, D. Kvasnicka, and J. Luitz, *WIEN2k: An Augmented Plane Wave Plus Local Orbitals Program for Calculating Crystal Properties* (University of Technology, Vienna, 2014).
37. P. E. Blochl, O. Jepsen, and O. K. Anderson, Phys. Rev. B: Condens. Matter **49**, 16223 (1994).
38. M. G. Brik and C.-G. Ma, Comput. Mater. Sci. **51**, 380 (2012).
39. A. L. Ivanovskii, V. P. Zhukov, and V. A. Gubanov, *Electronic Structure of Refractory Carbides and Nitrides* (Nauka, Moscow, 1990; Cambridge University Press, Cambridge, 1994).
40. J. Robertson, K. Xiong, and S. J. Clark, Thin Solid Films **496**, 1 (2006).
41. D. M. Roessler and W. C. Walker, Phys. Rev. **159**, 733 (1967).
42. S. Nisatharaju, R. Ayyappa, and D. Balamurugan, Asian J. Appl. Sci. **7**, 780 (2014).
43. R. A. de Groot, F. M. Mueller, P. G. van Engen, and K. H. J. Buschow, Phys. Rev. Lett. **50**, 2024 (1983).
44. R. Q. Wu, G. W. Peng, L. Liu, Y. P. Feng, Z. G. Huang, and Q. Y. Wu, Appl. Phys. Lett. **89**, 142501 (2006).
45. R. F. W. Bader, *Atoms in Molecules: A Quantum Theory* (Clarendon, Oxford, 1990).

Translated by O. Borovik-Romanova